Bright fluorescent nanoparticles for developing potential optical imaging contrast agents†

Guorong Sun,[ab] Mikhail Y. Berezin,*[b] Jinda Fan,[b] Hyeran Lee,[b] Jun Ma,[ab] Ke Zhang,[ab] Karen L. Wooley*[abc] and Samuel Achilefu*[b]

Received (in Cambridge, MA, USA) 13th October 2009, Accepted 8th December 2009
First published as an Advance Article on the web 8th February 2010
DOI: 10.1039/b9nr00304e

Fluorescent cross-linked nanoparticles with variable fluorophore loading amounts, locations, and particle sizes were synthesized from sequential one-pot functionalization/cross-linking of block copolymer micelles with amine-terminated dye and cross-linker molecules, *via* reductive amination and amidation. The fluorescence quantum yield and brightness of these nanoparticles were evaluated by steady-state and dynamic fluorescence methods. The results demonstrate that the quantum yield and brightness of the fluorescent nanoparticles correlated directly with the number of dyes/nanoparticle and the nanoparticle size. A strategy to increase the fluorescence brightness of nanoparticles with fluorescein and near-infrared dyes is proposed.

Introduction

During the past decades, *in vivo* fluorescence imaging has experienced a substantial growth with the "opening" of the near-infrared (NIR) window (wavelengths between 650 and 900 nm) of the electromagnetic spectrum.[1–7] By utilizing fluorescent probes, such as quantum dots,[8–10] fluorescent proteins,[11,12] and organic NIR dyes,[13–20] tissue autofluorescence and light attenuation associated with deep-tissue imaging are minimized, facilitating depth profiling of tissues to within a few centimetres by *in vivo* optical imaging.[4,5]

Among the organic NIR fluorophores (NIRFs), carbocyanine-based dyes are of particular interest, due to their high molar extinction coefficients (usually on the order of 10^5 M^{-1} cm^{-1}) and the tunability of their photo-physical properties.[19] The ease of functionalizing these NIRFs with bioactive ligands enables targeted imaging.[15,21–23] However, the *in vivo* application of cyanine dyes generally suffers from short blood circulation times and non-specific tissue/organ accumulations.[24–27] One approach to overcome these drawbacks is to encapsulate/couple cyanine dyes within/onto nanoscale platforms, which can provide protection and also impart "stealth" properties from the blood clearance systems.[14,28–45] The nanoscale platform can further be conjugated with multiple homo- or heterogeneous targeting agents to improve specificity by taking advantage of the interactions with cell-surface receptors. Furthermore, this approach may allow for "hybridization" of different probes within a single nanoparticle to provide multi-modal imaging, thereby improving the diagnostic accuracy.[42,46–50]

Nanoparticles (NPs) have been widely studied in molecular imaging. To date, cyanine NIRF-functionalized dendrimers,[37,48] silica NPs,[30,34,35,39,44,51,52] and natural/engineered viruses[29,33] have been reported. However, the design of fluorescent nanoparticles of small diameters is challenging because multiple fluorophores on the surface of a nanoparticle quench each other if they are located within the energy-transfer distance. Since the Förster radius for common fluorophores (1–10 nm)[53] is on the order of the nanoparticle diameter, care must be taken in synthesizing particles with desirable fluorescence properties. Herein, we investigated the optical properties of nanoparticles labelled with different numbers of common fluorescent dyes based upon fluorescein and cypate (a NIRF).[21] A synthetic procedure was developed for conjugating block copolymer-based nanoscale micellar assemblies with fluorescent molecules, followed sequentially *in situ* by covalent cross-linking of the polymers to afford robust nanoparticles having differential placement, number, and type of fluorescent chromophores. Investigation of their steady-state and dynamic optical properties, together with the synthetic efforts, allowed for optimization of these unique fluorescent nanoparticles to achieve a high level of fluorescence intensity.

Experimental

Materials

Cypate,[14] HL-800 (LS-277),[17] *S*-1-dodecyl-*S*′-(α,α′-dimethyl-α″-acetic acid)trithiocarbonate (DDMAT),[54] 4-(dimethy1amino)-pyridinium 4-toluenesulfonate (DPTS),[55] 4-vinylbenzaldehyde (VBA),[56] mPEG 2 kDa macro-chain transfer agent (macro-CTA),[57] and poly(ethylene oxide)-*block*-poly(*N*-acryloxy-succinimide)-*block*-polystyrene (PEO_{45}-*b*-$PNAS_{95}$-*b*-PS_{60})[58] were synthesized according to literature reports. Mono-methoxy-terminated mono-hydroxy poly(ethylene glycol) (mPEG 2 kDa and mPEG 5k Da, M_w = 2000 and 5000 Da, respectively, PDI = 1.06 and 1.07, respectively) were purchased from Intezyne

[a]*Department of Chemistry, Washington University in Saint Louis, Saint Louis, MO 63130, USA*
[b]*Department of Radiology, Washington University School of Medicine, Saint Louis, MO 63110, USA. E-mail: berezinm@mir.wustl.edu; achilefu@wustl.edu*
[c]*Department of Chemistry and Department of Chemical Engineering, Texas A&M University, College Station, TX 77842, USA. E-mail: wooley@mail.chem.tamu.edu*

† Electronic supplementary information (ESI) available: ^{1}H NMR spectra of block copolymer precursors, dynamic emission spectra of **CCFNP1**, DLS and TEM characterizations of **CCFNP8**, and UV–vis and fluorescence spectra of **CCFNP8**. See DOI: 10.1039/b9nr00304e

Technologies (Tampa, FL) and used without purification. Other reagents and solvents were purchased from Sigma-Aldrich (St. Louis, MO) and Acros Organics (Thermo Fisher Sci.) and were used without purification unless otherwise noted. Methylene chloride (CH_2Cl_2) was distilled from calcium hydride and stored under N_2. Nano-pure water was 18.0 MΩcm.

Measurements

^{1}H NMR spectra were recorded on a Varian 500 MHz spectrometer with CD_2Cl_2 and DMSO-d_6 as solvents and internal standards. Infrared spectra were obtained on a Perkin-Elmer Spectrum BX FT-IR system using diffuse reflectance sampling accessories with FT-IR Spectrum v2.00 software.

Absolute molecular weight and molecular weight distribution were determined by gel permeation chromatography (GPC). GPC was performed on a Waters 1515 HPLC system (Water Chromatography, Inc.), equipped with a Waters 2414 differential refractometer, a PD2020 dual-angle (15 and 90) light scattering detector (Precision Detectors, Inc.), and a three-column series PL gel 5 μm Mixed columns (Polymer Laboratories, Inc.). The eluent was anhydrous tetrahydrofuran (THF) with a flow rate of 1 mL min^{-1}. All instrumental calibrations were conducted using a series of nearly monodisperse poly(styrene) standards. Data were collected after an injection of 200 μL of polymer solution in THF (*ca.* 5 mg mL^{-1}) and then analyzed using the Discovery 32 software (Precision Detectors, Inc.).

The GPC with *N*,*N*-dimethylformamide (DMF) as a mobile phase was conducted on a Waters Chromatography, Inc. (Milford, MA) system equipped with an isocratic pump model 1515, a differential refractometer model 2414, and a two-column set of Styragel HR 4 and HR 4E 5 μm DMF 7.8 × 300 mm columns. The system was equilibrated at 70 °C in pre-filtered DMF containing 0.05 M LiBr, which served as polymer solvent and eluent (flow rate set to 1.00 mL min^{-1}). Polymer solutions were prepared at a concentration of *ca.* 3 mg mL^{-1} and an injection volume of 200 μL was used. Data collection and analysis was performed with Empower Pro software (Waters, Inc.). The system was calibrated with poly(ethylene glycol) standards (Polymer Laboratories, Amherst, MA) ranging from 615 to 442 800 Da.

Samples for transmission electron microscopy (TEM) measurements were diluted with a 1% phosphotungstic acid (PTA) stain (v/v, 1 : 1). Carbon grids were exposed to oxygen plasma treatment to increase the surface hydrophilicity. Micrographs were collected at 100 000× magnification and calibrated using a 41 nm polyacrylamide bead from NIST. The number average particle diameters (D_{av}) and standard deviations were generated from the analysis of a minimum of 150 particles from at least three different micrographs. The aggregation number (N_{aggr}) was calculated based upon the diameter measured from TEM by using the following equation:

$$N\text{aggr} = \frac{4\pi r^3 \rho}{3M_n} \times N_A \quad (1)$$

where r is the radius of the NP core domain, ρ is the density of poly-(4-vinyl benzaldehyde) (PVBA), M_n is the number-average molecular weight of PVBA block segment, and N_A is Avogadro's constant.

Hydrodynamic diameters (D_h) and size distributions for the nanoparticles in aqueous solutions were determined by dynamic light scattering (DLS). The DLS instrument consisted of a Brookhaven Instruments Ltd (Worcestershire, U.K.) system equipped with a model BI-200SM goniometer, a model BI-9000AT digital correlator, a model EMI-9865 photomultiplier, and a model 95-2 Ar ion laser (Lexel Corp.) operated at 514.5 nm. Measurements were made at 25 ± 1 °C. Scattered light was collected at a fixed angle of 90°. The digital correlator was operated with 522 ratio spaced channels, and initial delay of 5 μs, a final delay of 100 ms, and a duration of 8 min. A photomulitplier aperture of 400 μm was used and the incident laser intensity was adjusted to obtain a photon counting of between 150 and 200 kcps. Only measurements in which the measured and calculated baselines of the intensity autocorrelation function agreed to within 0.1% were used to calculate particle size. The calculations of the particle size distributions and distribution averages were performed with the ISDA software package (Brookhaven Instruments Co.), which employed single-exponential fitting, cumulants analysis, and CONTIN particle size distribution analysis routines. All experiments were repeated 5 times and the results are represented as intensity-averaged mean values with standard deviations between runs.

The fluorescence spectra of NPs were obtained at room temperature using a Varian Cary Eclipse and Fluorolog III fluorescence spectrophotometer. Fluorescence lifetime was measured using TCSPS method as described previously.[59] Briefly, the fluorescence decays were measured in aqueous media using λ_{ex} 460/λ_{em} 570 nm for fluorescein-based NPs or λ_{ex} 773/λ_{em} 820 nm for cypate-based NPs with bandpass 20 nm. In both measurements, a two-exponential decay analysis was applied.

For optical measurements, the fluorescein-based NPs were diluted with 0.1 M NaOH solution. NIR-based NPs were measured in PBS buffer at pH 7.2 (5 mM with 5 mM of NaCl). Samples were diluted to give the absorbance maximum value of 0.1 to avoid photon re-absorption.

The UV–vis absorption spectra of NPs were collected at room temperature using a Varian Cary 500 Bio UV–visible spectrophotometer in a quartz cuvette with a 10 mm light path.

The Förster radius of a homoFRET pair (R_0) was calculated using previously developed FRET calculator[37] from steady-state absorption and emission spectra using known equations:

$$R_0 = 0.211(k^2 n - 4\phi_D J(\lambda))^{1/6}\ \text{Å} \quad (2)$$

where k^2 is the orientation factor equal to 2/3 for randomly oriented fluorophores; n is the refractive index assumed to be 1.4 for biomolecules in aqueous solutions; Φ_D is the quantum yield of the donor; $J(\lambda)$ is the spectral overlap integral, which is calculated with the following equation:

$$J(\lambda) = \int_0^\infty F_D(\lambda)\varepsilon_A(\lambda)\lambda^4 d\lambda\ \text{M}^{-1}\ \text{cm}^{-1}\ \text{nm}^4 \quad (3)$$

where λ is the wavelength in nm; $F_D(\lambda)$ represents the normalized fluorescence intensity at wavelength λ; $\varepsilon_A(\lambda)$is molar absorptivity of the acceptor at a given wavelength.

Synthesis

Cypate diamine. To a solution of cypate (12.5 mg, 17.7 μmol) and 1-hydroxybenzotriazole (HOBt, 9.6 mg, 71 μmol) in DMF

was added *N*,*N*′-diisopropylcarbodiimide (DIC) (11.0 μL, 70.8 μmol) and the resulting mixture was stirred for 10 min at room temperature (rt). Boc-ethylene diamine (6.7 μL, 42 μmol) was then added and the resultant mixture was stirred overnight. After removal of DMF *in vacuo*, a cleavage mixture containing trifluoroacetic acid (TFA), H_2O, phenol, and thioanisole (85 : 5 : 5 : 5, v/v) was added and stirred for 1 h. The solvent was removed under reduced pressure and the crude product was washed with diethyl ether (3 × 5 mL) and purified by medium pressure chromatography with a C-18 reverse phase column (acetonitrile–water as eluent). A green solid was obtained as pure product (10.9 mg, 60.6% yield). MS (EI): 709.0 $(M + 1)^+$.

HL-800-amine (LS-277-amine). To a solution of HL-800 (10.4 mg, 11.2 μmol) and 2-(1*H*-7-azabenzotriazol-1-yl)-1,1,3,3-tetramethyl uronium hexafluorophosphate methanaminium (HATU, 6.4 mg, 17 μmol) in DMF was added diisopropylethyl amine (DIEA, 2.9 μL, 17 μmol) and the resulting mixture was stirred at rt for 10 min. Boc-ethylene diamine (2.1 μL, 20 μmol) was then added and the mixture was stirred overnight before being poured into 150 mL of diethyl ether to precipitate solid. Solid was then stirred in the cleavage mixture (TFA, H_2O, phenol, and thioanisole (85 : 5 : 5 : 5, v/v)) for 1 h. Diethyl ether was then added to the crude product to precipitate solid, washed with diethyl ether (3 × 5 mL) and further purified by medium pressure chromatography with a C-18 reverse phase column (acetonitrile–water as eluent). The solvents were evaporated to give HL-800-amine (3.18mg, 29.2% yield) as a green solid. MS (EI): 955.2 $(M + 1)^+$.

mPEG 5 kDa macro-CTA. To a solution of mPEG5000 (1.80 g, 0.36 mmol) in anhydrous CH_2Cl_2 (20 mL) was added DDMAT (0.20 g, 0.54 mmol) and dicyclohexylcarbodiimide (0.12 g, 0.54 mmol) and the reaction mixture was stirred for 10 min. After the additions of 4-di(methylamino)pyridine (13.2 mg, 0.11 mmol) and DPTS (68.6 mg, 0.22 mmol), the reaction mixture was further stirred for 20 h at rt. The resultant mixture was filtered with celite and the filtrate was stored at 4 °C overnight before additional filtration with celite to give the final concentration of *ca.* 8 mL.

The solid was precipitated by addition of anhydrous ethyl ether (150 mL) at 0 °C twice and the crude product obtained was further purified by flash column chromatography (2–3% MeOH–CH_2Cl_2, v/v) to afford mPEG 5 kDa macro-CTA as a yellow solid (1.2 g, 60% yield). ^{1}H NMR (500 MHz, CD_2Cl_2, δ): 0.88 (t, $J = 6.5$ Hz, 3H), 1.26 (m, 16H), 1.38 (t, $J = 6.5$ Hz, 2H), 1.66 (t, $J = 7.5$ Hz, 2H), 1.68 (s, 6H), 3.27 (t, $J = 7.2$ Hz, 2H), 3.33 (s, 3H), 3.40–3.80 (m, 440H), 4.21 (t, $J = 5.0$ Hz, 2H).

PEO_{45}-*b*-$PVBA_{18}$. To a 10 mL Schlenk flask equipped with a magnetic stir bar dried with flame under N_2 was added the mPEG 2 kDa macro-CTA (0.24 g, 0.10 mmol) in anhydrous DMF (2.5 mL). The reaction mixture was stirred for 1 h at rt to obtain a homogeneous solution. To this solution was added VBA (0.66 g, 5.0 mmol) and AIBN (3.2 mg, 20 μmol). The reaction flask was sealed and stirred for 10 min at rt. The reaction mixture was degassed through several cycles of freeze-pump-thaw. After the last cycle, the reaction mixture was stirred for 10 min at rt before immersing into a pre-heated oil bath at 75 °C to start the polymerization. After 4 h, the monomer conversion reached *ca.* 30% by analyzing aliquots collected through ^{1}H NMR spectroscopy. The polymerization was quenched by cooling the reaction flask with liquid N_2. CH_2Cl_2 (5.0 mL) was added to the reaction flask and the polymer was precipitated by addition of diethyl ether (300 mL) at 0 °C twice. The solid was collected, washed with 100 mL of cold ether, and dried *in vacuo* to afford the block copolymer precursor as a yellow solid (0.35 g, 80% yield based upon monomer conversion). ^{1}H NMR (500 MHz, CD_2Cl_2, δ): 0.88–1.24 (br, dodecyl Hs), 1.52–2.06 (br, PVBA backbone protons), 3.22 (br, SCH_2 of the chain terminus), 3.33 (s, mPEG terminal OCH_3), 3.34–3.78 (m, OCH_2CH_2O from the PEG backbone), 4.84 (br, 1H from the PVBA backbone benzylic terminus connected to the trithiocarbonate), 6.58–6.85 (br, Ar H), 7.33–7.62 (br, Ar H), 9.88 (br, CHO); ^{13}C NMR (150 MHz, DMSO-d_6, δ): 192.3, 151.3, 134.4, 129.4, 128.0, 69.8, 42.3, 40.4, 29.0; IR (KBr): 3433, 3000 − 2700, 1699, 1604, 1575, 1453, 1425, 1386, 1354, 1306, 1258, 1214, 1171, 1103, 1017, 951, 837, 726, 674, 552 cm^{-1}.

PEO_{113}-*b*-$PVBA_{46}$. To a 25 mL Schlenk flask equipped with a magnetic stir bar dried with flame under N_2 was added the mPEG 5 kDa macro-CTA (0.58 g, 0.11 mmol) in anhydrous DMF (7.0 mL). The reaction mixture was stirred for 1 h at rt to obtain a homogeneous solution. To this solution was added VBA (1.5 g, 11 mmol) and AIBN (3.4 mg, 21 μmol). The reaction flask was sealed and stirred for 10 min at rt. The reaction mixture was degassed through several cycles of freeze–pump–thaw. After the last cycle, the reaction mixture was stirred for 10 min at rt before being immersed into a pre-heated oil bath at 75 °C to start the polymerization. After 5.5 h, the monomer conversion reached *ca.* 47% by analyzing collected aliquots collected with ^{1}H NMR spectroscopy. The polymerization was quenched by cooling the reaction flask with liquid N_2. CH_2Cl_2 (5.0 mL) was added to the reaction flask and the solid was precipitated by addition of diethyl ether (300 mL) at 0 °C twice. The solid was collected, washed with 100 mL of cold ether, and dried under vacuum overnight to afford the block copolymer precursor as a yellow solid (0.92 g, 75% yield based upon monomer conversion). ^{1}H NMR (500 MHz, CD_2Cl_2, δ): 0.88–1.24 (br, dodecyl Hs), 1.52–2.06 (br, PVBA backbone protons), 3.22 (br, SCH_2 of the chain terminus), 3.33 (s, mPEG terminal OCH_3), 3.34–3.78 (m, OCH_2CH_2O from the PEG backbone), 4.84 (br, 1H from the PVBA backbone benzylic terminus connected to trithiocarbonate), 6.58–6.85 (br, Ar H), 7.33–7.62 (br, Ar H), 9.88 (br, CHO); ^{13}C NMR (150 MHz, DMSO-d_6, δ): 192.3, 151.3, 134.4, 129.4, 128.0, 69.8, 42.3, 40.4, 29.0; IR (KBr): 3433, 3000−2700, 1699, 1604, 1575, 1453, 1425, 1386, 1354, 1306, 1258, 1214, 1171, 1103, 1017, 951, 837, 726, 674, 552 cm^{-1}.

General procedure for construction of PEO-*b*-PVBA micelles

To a solution of PEO-*b*-PVBA block copolymer in DMF (*ca.* 1.0 mg mL^{-1}) was added an equal volume of water dropwise *via* a syringe pump at a rate of 15.0 mL h^{-1}, and the mixture was further stirred for 16 h at rt. The solution was then transferred to pre-soaked dialysis tubing (MWCO *ca.* 3500 Da) and dialyzed against water for 4 days to afford a solution of micelles.

General procedure for one-pot functionalization and cross-linking of PEO-*b*-PVBA micelles with fluorescein-5-thiosemicarbazide to construct core cross-linked fluorescent nanoparticles (CCFNP1–4)

To a solution of PEO-*b*-PVBA micelles in 10.0 mL of water, was added a solution of fluorescein-5-thiosemicarbazide (20 mol%, 2 mol%, 1 mol%, and 0.5 mol%, relative to the aldehyde residues, respectively) in DMF. The reaction mixture was allowed to stir for 2 h at rt in the dark. To this reaction mixture, was added a solution of 2,2′-(ethylenedioxy)-bis(ethylamine) (150 mol%, relative to the aldehyde residues) in water dropwise over 10 min and further stirred for 48 h at rt in the dark. $NaBH_3CN$ (200 mol%, relative to the aldehyde residues) in water was then added to the reaction solution and further stirred for 16 h at rt in the dark. Finally, the mixture was transferred to pre-soaked dialysis tubing (MWCO *ca.* 3500 Da) and dialyzed against 5.0 mM PBS (pH 7.2, with 5.0 mM NaCl) for 7 days to remove the small molecule byproducts and afford an aqueous solution of fluorescein-functionalized cross-linked nanoparticles.

General procedure for one-pot functionalization and cross-linking of PEO_{113}-*b*-$PVBA_{46}$ micelles with cypate-diamine to prepare core cross-linked fluorescent nanoparticles (CCFNP5–7)

To a solution of PEO_{113}-*b*-$PVBA_{46}$ micelles (2.7 mg of polymer, 11 μmol of aldehyde residues) in 10.0 mL of water, was added a solution of cypate-diamine (1 mol%, 0.5 mol%, and 0.2 mol%, relative to the aldehyde residues, respectively) in DMF. The reaction mixture was allowed to stir for 2 h at rt in the dark. To this reaction mixture was added a solution of 2,2′-(ethylenedioxy)-bis(ethylamine) (2.4 mg, 16 μmol) in water dropwise over 10 min and further stirred for 48 h at rt in the dark. $NaBH_3CN$ (1.4 mg, 22 μmol) in water was then added to the reaction solution and further stirred for 16 h at rt in the absence of light. Finally, the mixture was transferred to pre-soaked dialysis tubing (MWCO *ca.* 6000–8000 Da) and dialyzed against 5.0 mM PBS (pH 7.2, with 5.0 mM NaCl) for 7 days to remove the small molecule byproducts to afford an aqueous solution of functionalized and cross-linked nanoparticles.

Micellization of PEO_{45}-*b*-$PNAS_{95}$-*b*-PS_{60}

To a solution of PEO_{45}-*b*-$PNAS_{95}$-*b*-PS_{60} block copolymer in DMF (*ca.* 1.0 mg mL^{-1}), was added dropwise an equal volume of water *via* a syringe pump at a rate of 15.0 mL h^{-1}, and the mixture was further stirred for 1 h at rt before use for the following reactions.

Functionalization and cross-linking of PEO_{45}-*b*-$PNAS_{95}$-*b*-PS_{60} micelles with cypate-diamine or HL-800-amine to prepare shell cross-linked fluorescent Knedel-like nanoparticles (SCFK1–2)

To a solution of PEO_{45}-*b*-$PNAS_{95}$-*b*-PS_{60} micelles (4.8 mg of block copolymer precursor, 27 μmol of NAS residues) in 10 mL of DMF–H_2O (v:v = 1 : 1) at rt, was added the solution of cypate-diamine (38.3 μg, 0.054 μmol) or HL-800-amine (51.6 μg, 0.054 μmol) in 50 μL of DMF. The reaction mixture was allowed to stir for 2 h at rt in the dark. To this reaction mixture, was added a solution of 2,2′-(ethylenedioxy)-bis(ethylamine) (1.0 mg, 6.8 μmol) in water dropwise over 10 min and further stirred for 24 h at rt in the dark. The mixture was transferred to pre-soaked dialysis tubing (MWCO 6000–8000 Da) and dialyzed against 5.0 mM PBS (pH 7.2, with 5.0 mM NaCl) for 7 d to remove DMF, un-reacted crosslinker, and the small molecule byproducts to afford an aqueous solution of cross-linked nanoparticles.

One-pot functionalization and cross-linking of PEO_{113}-*b*-$PVBA_{46}$ micelle with HL-800-amine (CCFNP8)

To a solution of PEO_{113}-*b*-$PVBA_{46}$ micelles (2.7 mg of polymer, 11 μmol of aldehyde residues) in 10.0 mL of water, was added a solution of HL-800-amine (20.7 μg, 0.022 μmol) in DMF. The reaction mixture was allowed to stir for 2 h at rt in the absence of light. To this reaction mixture, was added a solution of 2,2′-(ethylenedioxy)-bis(ethylamine) (2.4 mg, 16 μmol) in water dropwise over 10 min and further stirred for 48 h at rt in the dark. $NaBH_3CN$ (1.4 mg, 22 μmol) in water was then added to the reaction solution and further stirred for 16 h at rt in the absence of light. Finally, the mixture was transferred to pre-soaked dialysis tubing (MWCO *ca.* 6000–8000 Da) and dialyzed against 5.0 mM PBS (pH 7.2, with 5.0 mM NaCl) for 7 days to remove the small molecule by-products and to afford an aqueous solution of functionalized and cross-linked nanoparticles.

Results and discussion

To construct fluorescent NPs, diblock copolymer (poly(ethylene oxide)-*block*-poly(4-vinyl benzaldehyde), PEO-*b*-PVBA) and triblock copolymer (poly(ethylene oxide)-*block*-poly(*N*-acryloxysuccinimide)-*block*-polystyrene, PEO-*b*-PNAS-*b*-PS) micelles were functionalized with fluorescein-5-thiosemicarbazide or amine-functionalized carbocyanine dyes through either reductive amination or amidation, respectively (Scheme 1). The PEO-*b*-PVBA diblock copolymers **I** (PEO_{45}-*b*-$PVBA_{18}$, $M_{n,\,NMR}$ = 4,700 Da, $M_{n,\,GPC}$ = 3,900 Da, PDI = 1.2, ESI† Fig. S1A) and **II** (PEO_{113}-*b*-$PVBA_{46}$, $M_{n,\,NMR}$ = 12,600 Da, $M_{n,\,GPC}$ = 12,400 Da, PDI = 1.4, ESI† Fig. S1B)[60] were used for construction of core functionalizable cross-linked nanoparticles (CCFNPs) while the PEO-*b*-PNAS-*b*-PS triblock copolymer **III** (PEO_{45}-*b*-$PNAS_{95}$-*b*-PS_{60}, $M_{n,\,NMR}$ = 18,400 Da, PDI = 1.2, ESI† Fig. S1C) was utilized as the precursor for shell cross-linked and shell fluorescently-labelled Knedel-like nanoparticles (SCFKs). All block copolymers were prepared by reversible addition-fragmentation chain transfer (RAFT) polymerization[61–64] based upon our previous reports.[57,58] PEO (M_w = 2000 and 5000 Da, respectively) was selected as the hydrophilic segment because of its good water solubility, well-known biocompatibility, and low immunogenic response,[65] and it was designed to occupy the corona of each of the nanostructures. PVBA was used as the hydrophobic and reactive segment for the core-cross-linked and fluorescently-labelled nanostructures, due to the broad reaction scope and the selectively-high reactivity of aldehydes under mild aqueous conditions. PNAS segments were utilized as pre-installed active esters along the central block segment of triblock copolymers for conjugation with amine-functionalized fluorophores within the shell layer of the shell cross-linked nanoparticles.

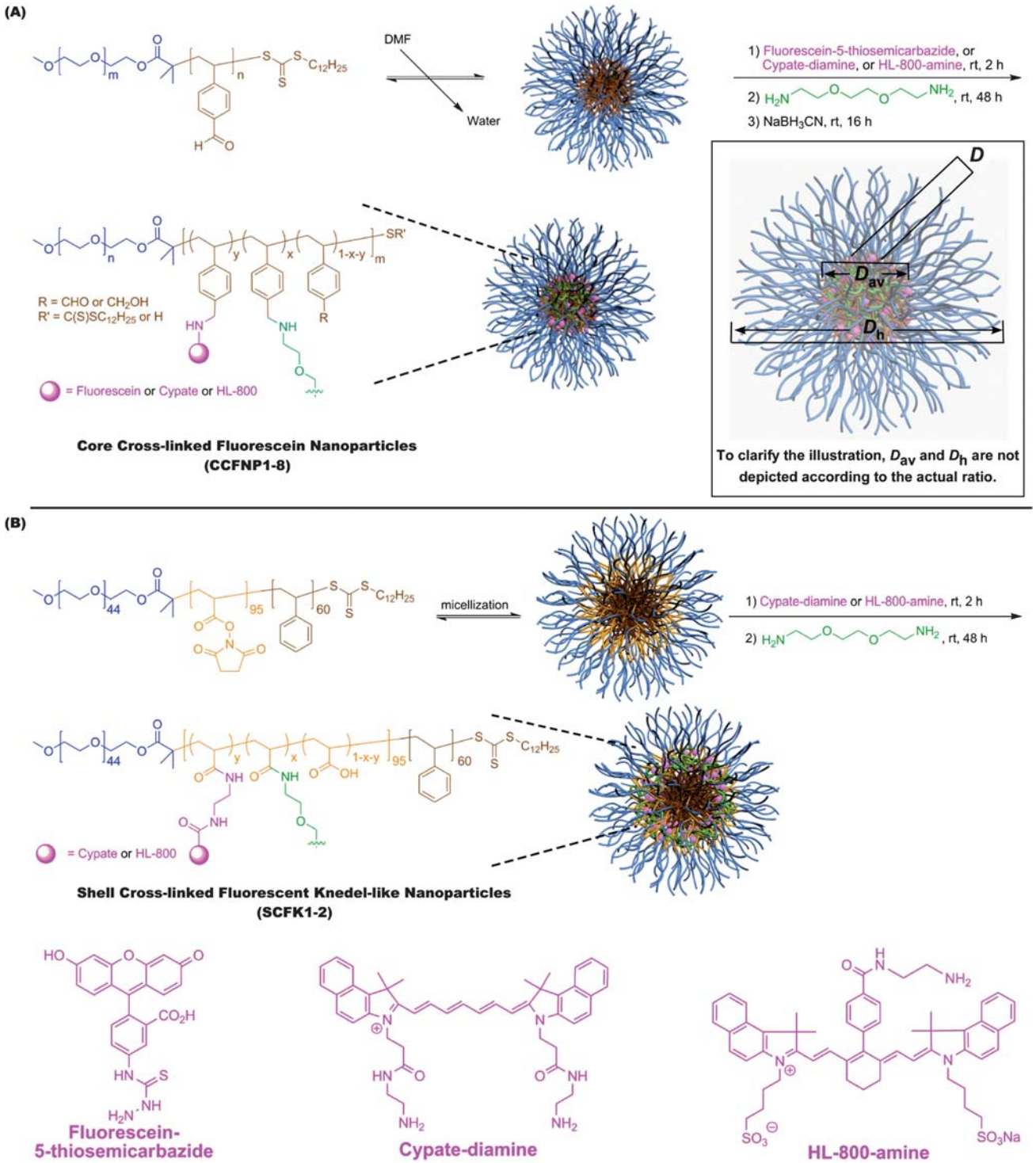

Scheme 1 Construction of fluorescent nanoparticles through reductive amination to afford core-crosslinked and core fluorescently-labelled nanoparticles (CCFNPs) (A) and through amidation to afford shell-crosslinked and shell fluorescently-labelled knedel-like nanoparticles (SCFKs) (B).

Aqueous assembly of block copolymers **I** and **II** followed conventional methods for micellization of amphiphilic block copolymers. A PEO selective solvent, *i.e.* water, was added to the solution of PEO-*b*-PVBA in organic solvent (DMF, *ca.* 1.0 mg mL^{-1}) at a rate of *ca.* 15 mL h^{-1} to induce the micellization and further stabilize the formed nanoscale-aggregates. The organic solvent was then removed by dialysis to afford PEO-*b*-PVBA micelles with PEO shells and PVBA core domains. The uniformity and narrow size distribution of the assembled micelles were demonstrated through a combination of DLS and TEM (Fig. 1). The DLS measurements showed that these micelles had an intensity-averaged hydrodynamic diameter ($D_{h,\ intensity}$) of 23 ± 2 nm (from PEO_{45}-*b*-$PVBA_{18}$) and 26 ± 2 nm (from PEO_{113}-*b*-$PVBA_{46}$), respectively. TEM micrographs revealed their globular

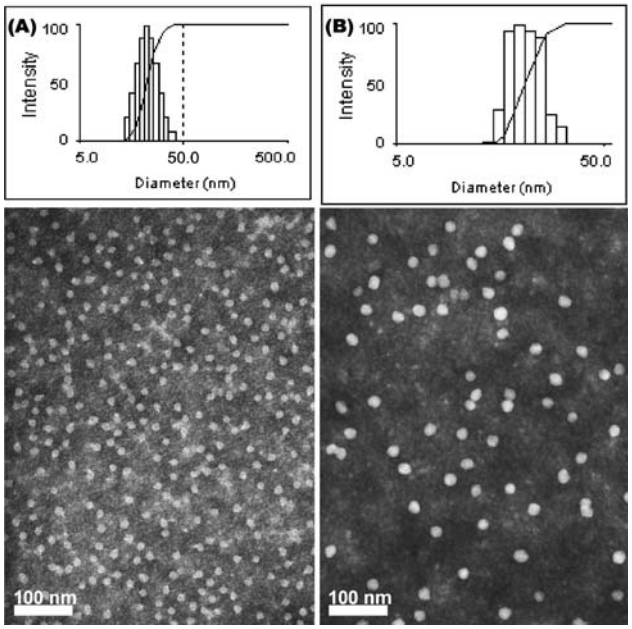

Fig. 1 Characterization of PEO-*b*-PVBA micelles. Intensity-average weighted hydrodynamic diameter distribution histograms by DLS (top) and TEM micrograph (bottom, stained with PTA): (A) PEO_{45}-*b*-$PVBA_{18}$ micelles; (B) PEO_{113}-*b*-$PVBA_{46}$ micelles.

shapes with an average core domain diameter (D_{av}) of 13 ± 1 nm and 19 ± 1 nm, respectively, depending upon the length of PVBA block segment.

One-pot chemical functionalization, with fluorescein-5-thiosemicarbazide, and sequential cross-linking, with diamine cross-linker, of the PEO_{45}-*b*-$PVBA_{18}$ micelles were achieved by our previously published procedure (Scheme 1A).[57] Similar to our previous findings,[57] buffer solutions with certain ionic strength (pH 7.2, 5 mM PBS with 5 mM of NaCl in this study) were found to be required to prevent the precipitation of the cross-linked nanoparticles. For **CCFNP1** (prepared with a feeding ratio of fluoresceins/aldehydes = 0.2 : 1), the DLS ($D_{h,\ intensity}$ = 21 ± 1 nm) and TEM (D_{av} = 13 ± 1 nm) characterizations of the functionalized cross-linked NPs showed no obvious morphology, size, and size distribution changes (Fig. 2A), compared with the micelle precursors (Fig. 1A). UV–vis measurement of the fluorescein-NP solutions revealed that a slight red-shift of *ca.* 8 nm (Fig. 2E left) occurred for the maximum absorption peak (λ_{max}, 496 nm for the fluorescein-functionalized NPs *vs.* 488 nm for the unconjugated fluorescein), which might be related to the change of fluorescein local environment before and after incorporation into the nanostructure. Although the thiosemicarbazide is a strong nucleophile, the coupling efficiency of fluorescein into the NPs was only *ca.* 12%. This might be associated with the low accessibility of hydrophilic fluorescein to the hydrophobic benzaldehyde functionalities (packed inside the hydrophobic core domain of the micelles).

A steady-state fluorescence spectrum of the diluted NP solution was recorded at the excitation wavelength of 450 nm over the range of 465–650 nm (Fig. 2E). Compared with the spectrum of the fluorescein small molecule, much lower fluorescence emission intensity of the **CCFNP1** sample (200-fold drop at the same concentration magnitude) was observed. The decrease in fluorescence of fluorescein attached to nanoparticles could be attributed to self-quenching *via* non-radiative energy transfer mechanism (homoFRET) between fluorophores in close proximity. We hypothesized that incorporating *ca.* 150 dye molecules into a confined space with *ca.* 13 nm diameter placed the fluorophores within distances much shorter than the Förster radius R_0 – the distance at which 50% of energy transfers to another fluorophore (*vide infra*).

The R_0 measurement for fluorescein using steady-state spectra (see the Experimental section) provided a homoFRET distance of 4.7 nm, similar to the literature value (4.4 nm).[66] The average distance between two fluorescein moieties on the NPs (r) was calculated from both steady-state and dynamic emission spectra by using the following equations:

$$r(\phi) = R_D\left(\frac{\phi_{da}}{\phi_d - \phi_{da}}\right)^{\frac{1}{6}} \text{nm for steady-state emission} \quad (4)$$

where ϕ_{da} is the quantum yield of the donor in the presence of acceptor, and ϕ_d is the quantum yield of the donor in the absence of acceptor, and

$$r(\tau) = R_D\left(\frac{\tau_{da}}{\tau_d - \tau_{da}}\right)^{\frac{1}{6}} \text{nm for dynamic emission} \quad (5)$$

where τ_{da} represents the fluorescence lifetime of the donor in the presence of acceptor, and τ_d is the fluorescence lifetime of the donor in the absence of acceptor.

Ideally, both methods provide the same results, however, the distances obtained from the lifetime measurements were consistently higher than those from quantum yield calculations (Table 1). Such discrepancy in the results suggests the presence of mechanisms other than FRET for quenching. For example, at high fluorophore concentrations, photon re-absorption and subsequent photon re-emission can increase the fluorescence lifetime values significantly. Accordingly, the local concentration of fluorescein within the nanoparticles is rather high, which might create an environment favourable for re-absorption. This condition is supported by the fact that at lower conjugation number, $r(\phi)$ and $r(\tau)$ values become closer. Another possible explanation for the discrepancy in results may be attributed to the fact that the relative fluorescence quantum yield used in this work did not take into account that the molar absorptivity of fluorescein is highly sensitive to a substitution pattern as well as to a polarity of the solvent. However, the measurement of molar absorptivity in systems like nanoparticles is challenging because it requires the knowledge of exact nanoparticle compositions. Finally, in addition to the homoFRET, other non-energy transfer quenching mechanisms, such as dynamic and static quenching have to be taken into account.

We have previously established a semi-quantitative model for evaluation of the PEG surface coverage density across a nanoparticle.[67] Because only ~2.5% of the VBA units were actually "decorated" with fluorescein, the fluorescein molecules should be attached to the most accessible VBA units, *i.e.* benzaldehydes around the periphery of the core domain. Therefore, the previous model could be easily revised to estimate the distance between adjacent fluorescein molecules (depicted as D in the Scheme 1 insertion) through the following equation:

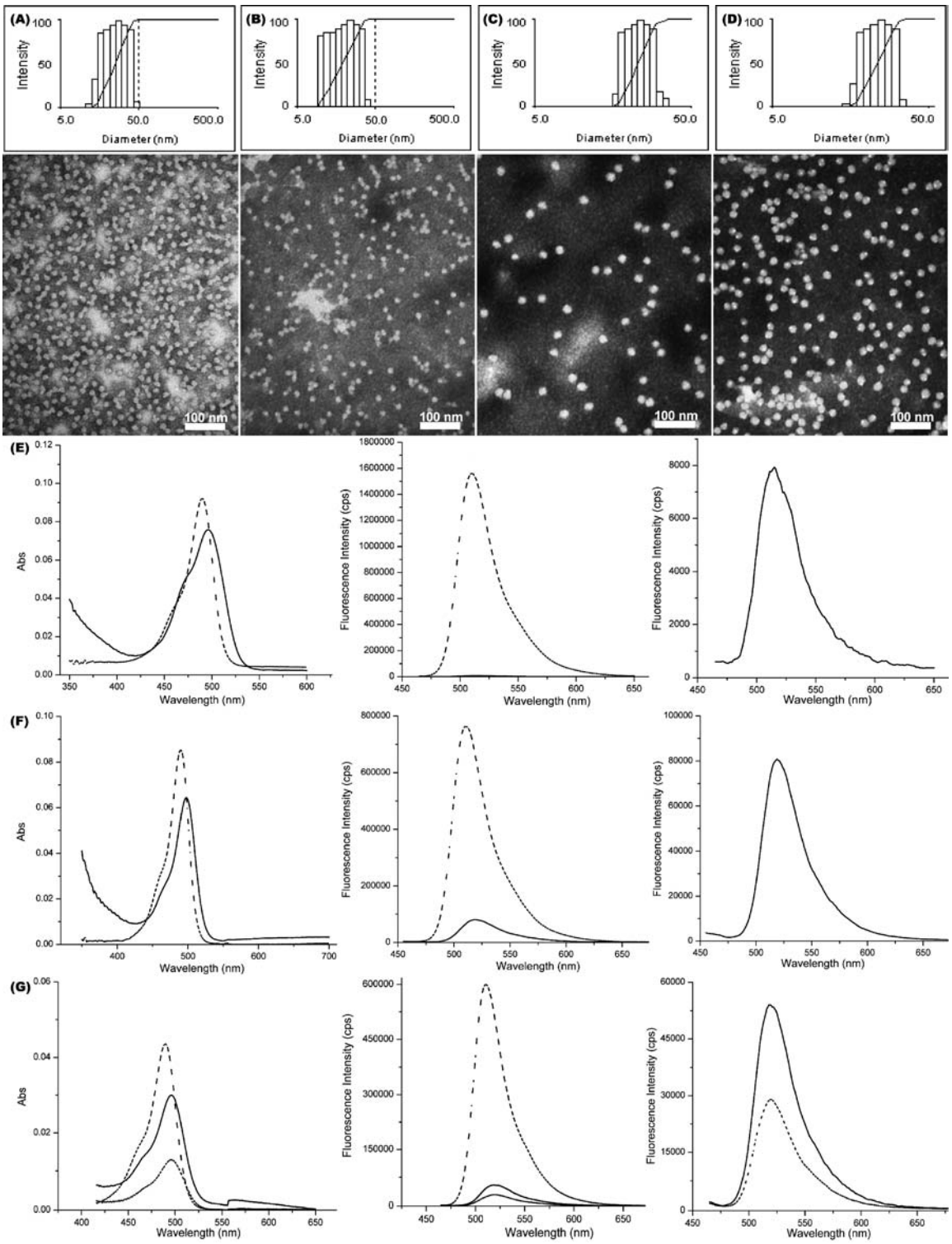

Fig. 2 Characterizations of **CCFNP1–4**. (A–D) Intensity-average weighted hydrodynamic diameter distribution by DLS (top) and TEM micrograph (bottom, stained with PTA) of **CCFNP1–4**, respectively. (E) UV–vis (left) and fluorescence emission (middle and right) spectra of **fluorescein** (dashed) and **CCFNP1** (solid). (F) UV–vis (left) and fluorescence emission (middle and right) spectra of **fluorescein** (dashed) and **CCFNP2** (solid). (G) UV–vis (left) and fluorescence emission (middle and right) spectra of **fluorescein** (dashed), **CCFNP3** (short dashed) and **CCFNP4** (solid).

Table 1 Calculated distance between two adjacent fluorescein moieties incorporated into nanoparticles and the optical characteristics of core cross-linked fluorescent nanoparticles

Sample	$D_{h,\ intensity}$[a]/nm	D_{av}[b]/nm	N_{agg}[c]	N[d]	D[e]/nm	τ[f]/ns	$r(\tau)$[g]/nm	ϕ[h]	$r(\phi)$[i]/nm	B[j]$\times 10^{-3}$ M^{-1} cm^{-1}
Fluorescein	—	—	—	—	—	3.92	—	0.79	—	62.4
CCFNP1	21 ± 1	13 ± 1	350	150	1.88	2.01	4.76	0.005	2.01	59.3
CCFNP2	22 ± 2	13 ± 1	350	15	5.95	2.97	5.65	0.088	3.30	104.3
CCFNP3	24 ± 2	19 ± 1	430	15	8.69	3.33	6.23	0.233	4.04	276.1
CCFNP4	24 ± 2	19 ± 1	430	30	6.15	3.11	5.84	0.215	3.96	509.6

[a] Intensity-averaged hydrodynamic diameter. [b] Average core domain diameter. [c] Nanoparticle aggregation number. [d] Dyes per nanoparticle, calculated based upon $\varepsilon = 76\,000$ M^{-1} cm^{-1}. [e] Calculated distance between two adjacent fluorophores within nanoparticle. [f] Fluorescence average lifetime. Complex multiexponential decay of nanoparticles (see the beginning of the decay shown in ESI† Fig. S2) suggested the presence of many distances between fluorescein moieties. [g] Distance between two fluorophores based on lifetime measurement [eqn (5)]. [h] Fluorescence quantum yield. [i] Distance between two fluorophores based on steady-state data [eqn (4)]. [j] Fluorescence brightness [see eqn (8)].

$$D = \sqrt{\frac{\pi(D_{av})^2}{N}}\ \text{nm} \tag{6}$$

where N denotes the number of fluorophores per NP (obtained from the number of fluorophores per polymer chain and the aggregation number of polymer chains estimated to be within each nanoparticle, see the Experimental section for details), and D_{av} is the average diameter of the core domain of the nanoparticles. The results of our calculations are given in Table 1.

According to a known Förster equation [eqn (7)],[66] no energy transfer and therefore no quenching would occur if the distance between two fluoresceins (r) exceeds 9 nm ($E_T = 0.02\%$).

$$E_T = \frac{R_0^6}{R_0^6 + r^6} \tag{7}$$

For **CCFNP1**, the calculated distances between two fluorescein molecules, both from eqn (6) (1.88 nm) and from the experimental calculations (2.00 nm from steady-state [eqn (4)] and 4.75 nm from dynamic [eqn (5)] measurements, respectively), were far below 9 nm. This condition would result in substantial self-quenching and low brightness of the nanoparticles ($B = 59.3 \times 10^3$ M^{-1} cm^{-1} for **CCFNP1**). Thus, 150 fluorescein moieties had the brightness of a single fluorescein molecule, which is certainly not satisfactory.

$$B = \varepsilon\phi N,\ M^{-1}\ cm^{-1} \tag{8}$$

where ε is the molar absorptivity (was approximated to ~76 000 M^{-1} cm^{-1} and ~200 000 M^{-1} cm^{-1} for, respectively, fluorescein at 488 nm, cypate at 780 nm, and HR-800 at 800 nm, actual molar absorptivity was not determined), ϕ is the fluorescence quantum yield, and N represents the number of fluorophores per nanoparticle.

To improve the brightness of fluorescein-incorporated nanoparticles, the number of fluorophores per nanoparticle should be decreased to overcome the homoFRET quenching. Accordingly, **CCFNP2** with *ca.* 15 fluoresceins per NP was prepared from the same block copolymer micelle as **CCFNP1**, maintaining similar size ($D_{h,\ intensity} = 22 \pm 2$ nm and $D_{av} = 13 \pm 1$ nm) and size distribution (Fig. 2B).[68] The quantum yield was significantly improved by a factor of 18 (Table 1) due to the increase of the distance between fluorescein moieties, as calculated from the experimental data [eqns (4) and (5)] and from eqn (6) (Table 1). However, the overall improvement of fluorescence brightness was only marginal (1.043×10^5 M^{-1} cm^{-1}).

A simple calculation (not shown here) estimates a maximum number of 5 fluoresceins per nanoparticle for the PEO_{45}-*b*-$PVBA_{18}$ system (13 nm diameter core) to allow at least 9 nm distance between fluoresceins and to further eliminate possible homoFRET quenching. With such a small loading, even in the absence of any other quenching mechanisms the fluorescence brightness cannot exceed a theoretical value of 3×10^5 M^{-1} cm^{-1}. To improve the overall brightness of fluorescent nanoparticles without inducing homoFRET quenching, it is advantageous to use nanoparticles with larger cores to allow an increased number of fluorophores per nanoparticle as indicated in eqn (6). Accordingly, **CCFNP3** and **CCFNP4** with larger core sizes (19 *vs.* 13 nm, Fig. 2C and 2D, respectively) were prepared from PEO_{113}-*b*-$PVBA_{46}$ block copolymer micelles.[69]

With a core size of 19 nm and 15 fluorescein molecules/NP, the calculated D for **CCFNP3** was 8.69 nm, which is close to the target 9 nm cut-off range. In fact, only 15.7% of the absorbed energy was non-radiatively transferred between fluorescein moieties (based on lifetime measurement). As a result, the quantum yield of **CCFNP3** increased to 0.233, a 2.5-fold enhancement compared with **CCFNP2** with brightness of 276.1 x10^3 M^{-1} cm^{-1}. For **CCFNP4**, which bears 30 fluoresceins per particle, a small drop of quantum yield (0.215) was observed. This is likely due to the relative proximity between fluorophores ($D = 6.15$ nm). However, the slightly decreased quantum yield was compensated by the higher number of fluorophores, rendering its overall fluorescence intensity 190% as large as that of **CCFNP3** (Fig. 2G, right). The calculated brightness of 509.6×10^3 M^{-1} cm^{-1} is nearly an order of magnitude higher than that for a single fluorescein molecule.

The PEO_{113}-*b*-$PVBA_{46}$ micelle system and the optimized stoichiometry of fluorescein loading (less than 1 mol%, relative to the aldehydes) were then extended to construct NIR fluorescent nanoparticles using cypate (Scheme 1A). **CCFNP5–7** with *ca.* 70, 45, and 10 cypates per particle, respectively, were synthesized and evaluated by photophysical methods (Fig. 3). Coupling yields using cypate improved to ~36% to 47% compared with the fluoresceins at ~12% to 15%. This improvement could be attributed to the fact that cypate is more hydrophobic than fluorescein and interacts favourably with the hydrophobic PVBA core.

The calculated distances derived from eqn (6) between neighbouring cypate molecules for **CCFNP5–7** were 4.02 nm, 5.02 nm,

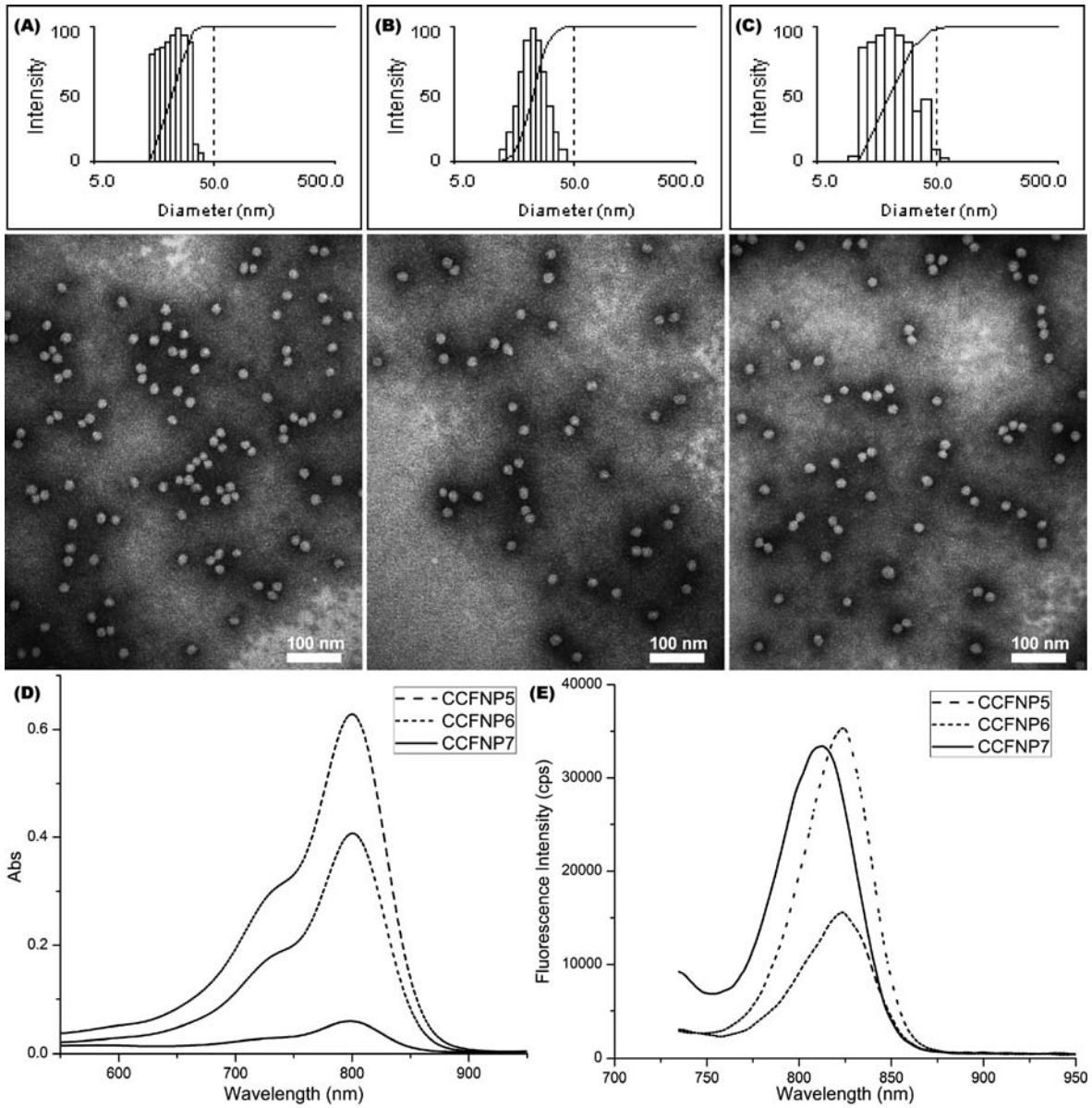

Fig. 3 (A–C) Intensity-average weighted hydrodynamic diameter distribution histogram by DLS (top) and TEM micrograph (bottom, stained with PTA) of **CCFNP5**, **CCFNP6**, and **CCFNP7**, respectively. (D–E) UV–vis and fluorescence profiles of **CCFNP5** (dashed), **CCFNP6** (short dashed), and **CCFNP7** (solid), respectively.

and 10.65 nm, respectively (Table 2). The brightness values significantly improved from 4.2×10^3 M^{-1} cm^{-1} for a single cypate molecule to 3.6×10^4 M^{-1} cm^{-1} for **CCFNP6**. However, a low quantum yield of 0.004 was obtained. For **CCFNP7**, with a higher *D* value of over 10 nm, an enhanced quantum yield value of 0.019 was observed, which is very close to the free cypate in water (0.021), as expected. However, due to the lower number of fluorophores on the nanoparticles, the overall brightness (3.8×10^4 M^{-1} cm^{-1}) remained similar to **CCFNP6**.

Previously, we have shown that the fluorescence lifetime of cyanine dyes, such as cypate, is significantly affected by the polarity of the media.[59] To further explore the relationship between the brightness of the fluorescent nanoparticles with the locations of the fluorophores, NIRF shell cross-linked fluorescent

Table 2 Physical and optical characteristics of NIR fluorescent nanoparticles from the PEO_{113}-*b*-$PVBA_{46}$ system

Sample	$D_{h,\ intensity}$[a]/ nm	D_{av}[b]/ nm	N_{agg}[c]	N[d]	D[e]/ nm	ϕ[f]	B[g] $\times 10^{-3}$ M^{-1} cm^{-1}
Cypate	—	—	—	—	—	0.021	4.2
CCFNP5	23 ± 1	19 ± 1	430	70	4.02	0.001	14.0
CCFNP6	23 ± 1	19 ± 1	430	45	5.02	0.004	36.0
CCFNP7	22 ± 2	19 ± 1	430	10	10.65	0.019	38.0

[a] Intensity-averaged hydrodynamic diameter. [b] Average core domain diameter. [c] Nanoparticle aggregation number. [d] Dyes per nanoparticle, calculated based upon $\varepsilon = 200\,000$ M^{-1} cm^{-1}. [e] Calculated distance between two adjacent cypates within nanoparticle. [f] Fluorescence quantum yield, relative to indocyanine green (ICG) in methanol (quantum yield = 0.09). [g] Fluorescence brightness.

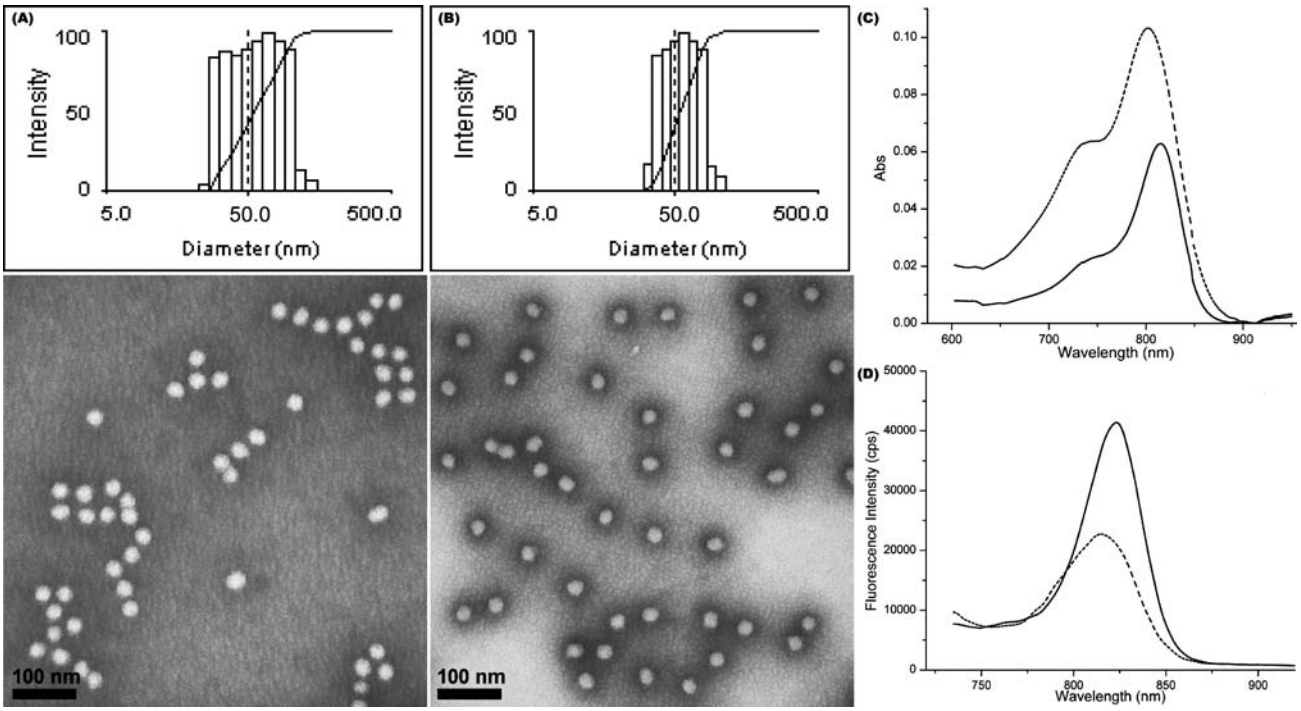

Fig. 4 Physical and photo-physical properties of shell cross-linked NIR fluorescent nanoparticles. (A–B) Intensity-average weighted hydrodynamic diameter distribution histograms by DLS (top) and TEM micrographs (bottom, stained with PTA) of **SCFK1** and **SCFK2**, respectively. (C–D) UV–vis and fluorescence profiles of **SCFK1** (dashed) and **SCFK2** (solid), respectively.

Knedel-like nanoparticles (NIR-SCFKs, **SCFK1–2**) were prepared, in which carbocyanine molecules having differing hydrophobicities/hydrophilicities (Cypate for **SCFK1** and HL-800 for **SCFK2**, respectively) were distributed throughout the hydrophilic shell domain (Scheme 1B). These particles showed relatively narrow size distributions and globular shape, as observed through DLS and TEM (Fig. 4A–B). The photophysical characteristics of **SCFK1** and **SCFK2** are summarized in Table 3.

At a similar cypate loading capacity as **CCFNP6**, **SCFK1** showed similar quantum yield and brightness. NIR-SCFKs with improved optical characteristics were achieved when cypate was replaced with HL-800 at a loading capacity of 20 HL-800s/SCFK (**SCFK2**). The *D* value for **SCFK2** was between the range of 12 nm to 22 nm. The quantum yield of **SCFK2** (0.036, Table 3) was enhanced by a factor of 7 and the overall fluorescence brightness gained a 3.6-fold increase relative to **SCFK1**. Encouraged by the high brightness, HL–800 was further introduced into the PEO_{113}-*b*-$PVBA_{46}$ system to afford **CCFNP8** (Scheme 1A) bearing 5 dyes in the core of each NP while maintaining a similar size as those of **CCFNP5–7** (ESI† Fig. S3A, $D_{h,\ intensity} = 22 \pm 1$ nm and $D_{av} = 19 \pm 1$ nm) and comparable inter-dye spacing, similar to **SCFK2** ($D = 15$ nm). Unfortunately, a dramatic decrease in quantum yield from 0.036 to 0.002 resulted in very low (2×10^3 M^{-1} cm^{-1}) brightness of these core-cross-linked and HL-800-labelled nanoparticles. The mechanism for such lower fluorescence emission is unclear.

Table 3 Characterizations and optical characteristics of NIR-SCFKs from PEO_{45}-*b*-$PNAS_{95}$-*b*-PS_{60} micelles

Sample	$D_{h,\ intensity}$[a]/ nm	D_{av}[b]/ nm	N_{agg}[c]	N[d]	ϕ[e]	B[g] $\times 10^{-3}$ M^{-1} cm^{-1}
SCFK1	59 ± 3	30 ± 1	1450	40	0.005	40.0
HL-800	—	—	—	—	0.088[f]	17.6
SCFK2	56 ± 2	30 ± 1	1450	20	0.036	144.0

[a] Intensity-averaged hydrodynamic diameter. [b] Average core domain diameter. [c] Nanoparticle aggregation number. [d] Dyes per nanoparticle, calculated based upon $\varepsilon = 200\,000$ M^{-1} cm^{-1}. [e] Fluorescence quantum yield. [f] Relative to ICG in methanol (quantum yield = 0.09). [g] Fluorescence brightness.

Conclusions

In summary, we have prepared unique core or shell-cross-linked and fluorescently-labelled nanomaterials and studied their photo-physical properties. Fluoresceins or NIR carbocyanine (cypate and HL-800) dyes were incorporated at different stoichiometric loadings and within different regions of the nanostructures to modify the local environment and inter-dye spacings. The brightness of the fluorescent nanoparticles was evaluated by varying the fluorophore loading capacity and location within nanoparticles of different sizes. As a result of optimization, we successfully prepared nanoscale agents with fluorescent brightness values that are ~10-fold higher than those of free fluorescein or NIR dye molecules. Such bright fluorescent nanoparticles could be utilized in a variety of biological applications, particularly in fluorescence microscopy and *in vivo* imaging for significant contrast enhancement.

Acknowledgements

This material is based upon work supported partially by the National Heart, Lung and Blood Institute of the National Institutes of Health as a Program of Excellence in

Nanotechnology (HL080729), and by the National Institutes of Health grant number 1R01EB008111. The authors thank Mr. G. M. Veith for his kind assistance with TEM imaging; and Dr J. Kao for assistance with NMR measurements.

Notes and references

1 J. V. Frangioni, *Curr. Opin. Chem. Biol.*, 2003, **7**, 626–805.
2 V. Ntziachristos, J. Ripoll, L. V. Wang and R. Weissleder, *Nat. Biotechnol.*, 2005, **23**, 313–320.
3 K. Licha and C. Olbrich, *Adv. Drug Delivery Rev.*, 2005, **57**, 1087–1108.
4 V. Ntziachristos, *Annu. Rev. Biomed. Eng.*, 2006, **8**, 1–33.
5 J. Rao, A. Dragulescu-Andrasi and H. Yao, *Curr. Opin. Biotechnol.*, 2007, **18**, 17–25.
6 V. Ntziachristos, *Genomic and Personalized Medicine*, 2009, 524–531.
7 B. M. W. Tsui and D. L. Kraitchman, *J. Nucl. Med.*, 2009, **50**, 667–670.
8 X. Gao, Y. Cui, R. M. Levenson, L. W. K. Chung and S. Nie, *Nat. Biotechnol.*, 2004, **22**, 969–976.
9 X. Michalet, F. F. Pinaud, L. A. Bentolila, J. M. Tsay, S. Doose, J. J. Li, G. Sundaresan, A. M. Wu, S. S. Gambhir and S. Weiss, *Science*, 2005, **307**, 538–544.
10 M. K. So, C. Xu, A. M. Leoning, S. S. Gambhir and J. Rao, *Nat. Biotechnol.*, 2006, **24**, 339–343.
11 R. M. Hoffman, *Nat. Rev. Cancer*, 2005, **5**, 796–806.
12 N. Shaner, P. A. Steinbach and Y. T. Tsien, *Nat. Methods*, 2005, **2**, 905–909.
13 S. Achilefu, *Technol. Cancer Res. Treat.*, 2004, **3**, 393–410.
14 Y. Ye, S. Bloch and S. Achilefu, *J. Am. Chem. Soc.*, 2004, **126**, 7740–7741.
15 Z. Cheng, Y. Wu, Z. Xiong, S. S. Gambhir and X. Chen, *Bioconjugate Chem.*, 2005, **16**, 1433–1441.
16 W. Pham, Z. Medarova and A. Moore, *Bioconjugate Chem.*, 2005, **16**, 735–740.
17 H. Lee, J. C. Mason and S. Achilefu, *J. Org. Chem.*, 2006, **71**, 7862–7865.
18 A. Masotti, P. Vicennati, F. Boschi, L. Calderan, A. Sbarbati and G. Ortaggi, *Bioconjugate Chem.*, 2008, **19**, 983–987.
19 L. Strekowski, *Heterocyclic Polymethine Dyes: Synthesis, Properties and Applications*, Springer, Berlin/Heidelberg, 2008.
20 Z. Zhang, M. Y. Berezin, J. L. F. Kao, A. d'Avignon, M. Bai and S. Achilefu, *Angew. Chem., Int. Ed.*, 2008, **47**, 3584–3587.
21 S. Achilefu, R. B. Dorshow, J. E. Bugal and R. Rajagopalan, *Invest. Radiol.*, 2000, **35**, 479–485.
22 S. Achilefu, S. Bloch, M. A. Markiewicz, T. Zhong, Y. Ye, R. B. Dorshow, B. Chance and K. Liang, *Proc. Natl. Acad. Sci. U. S. A.*, 2005, **102**, 7976–7981.
23 Y. Ye, S. Bloch, B. Xu and S. Achilefu, *J. Med. Chem.*, 2006, **49**, 2268–2275.
24 W. West and S. Pearce, *J. Phys. Chem.*, 1965, **69**, 1894–1903.
25 P. Ott, *Pharmacol. Toxicol.*, 1998, **83**, 1–48.
26 V. Saxena, M. Sadoqi and J. Shao, *J. Pharm. Sci.*, 2003, **92**, 2090–2097.
27 J. A. Cardillo, R. Jorge, R. A. Costa, S. M. Nunes, D. Lavinsky, B. D. Kuppermann, A. C. Tedesco and M. E. Farah, *Br. J. Ophthalmol.*, 2008, **92**, 276–280.
28 V. Saxena, M. Sadoqi and J. Shao, *J. Photochem. Photobiol., B*, 2004, **74**, 29–38.
29 C. Wu, H. Barnhill, X. Liang, Q. Wang and H. Jiang, *Opt. Commun.*, 2005, **255**, 366–374.
30 T. Deng, J.-S. Li, J.-H. Jiang, G.-L. Shen and R.-Q. Yu, *Adv. Funct. Mater.*, 2006, **16**, 2147–2155.
31 K. Kim, M. Lee, H. Park, J.-H. Kim, S. Kim, H. Chung, K. Choi, I.-S. Kim, B. L. Seong and I. C. Kwon, *J. Am. Chem. Soc.*, 2006, **128**, 3490–3491.
32 P. Sharma, S. Brown, G. Walter, S. Santra and B. Moudgil, *Adv. Colloid Interface Sci.*, 2006, **123–126**, 471–485.
33 C. M. Soto, A. S. Blum, G. J. Vora, N. Lebedev, C. E. meador, A. P. Won, A. Chatterji, J. E. Johnson and B. R. Ratna, *J. Am. Chem. Soc.*, 2006, **128**, 5184–5189.
34 X. He, J. Chen, K. Wang, D. Qin and W. Tan, *Talanta*, 2007, **72**, 1519–1526.
35 Z. Yang, S. Zheng, W. J. Harrison, J. Harder, X. Wen, J. G. Gelovani, A. Qiao and C. Li, *Biomacromolecules*, 2007, **8**, 3422–3428.
36 J. Yu, M. A. Yaseen, B. Anvari and M. S. Wong, *Chem. Mater.*, 2007, **19**, 1277–1284.
37 A. Almutairi, W. J. Akers, M. Y. Berezin, S. Achilefu and J. M. J. Fréchet, *Mol. Pharmacol.*, 2008, **5**, 1103–1110.
38 E. I. Altınoğlu, T. J. Russin, J. M. Kaiser, B. M. Barth, P. C. Eklund, M. Kester and J. H. Adair, *ACS Nano*, 2008, **2**, 2075–2084.
39 J. F. Bringley, T. L. Penner, R. Wang, J. F. Harder, W. J. Harrison and L. Buonemani, *J. Colloid Interface Sci.*, 2008, **320**, 132–139.
40 W. Chen, *J. Nanosci. Nanotechnol.*, 2008, **8**, 1019–1051.
41 S. Lee, E.-J. Cha, K. Park, S.-Y. Lee, J.-K. Hong, I.-C. Sun, S. Y. Kim, K. Choi, I. K. Kwon, K. Kim and C.-H. Ahn, *Angew. Chem., Int. Ed.*, 2008, **47**, 2804–2807.
42 Y. T. Lim, Y.-W. Noh, J. H. Han, Q.-Y. Cai, K.-H. Yoon and B. H. Chung, *Small*, 2008, **4**, 1640–1645.
43 V. B. Rodriguez, S. M. Henry, A. S. Hoffman, P. S. Stayton, X. Li and S. H. Pun, *J. Biomed. Opt.*, 2008, **13**, 014025–25.
44 A. A. Burns, J. Vider, H. Ow, E. Herz, O. Penate-Medina, M. Baumgart, S. M. Larson, U. Wiesner and M. Bradbury, *Nano Lett.*, 2009, **9**, 442–448.
45 A.-K. Kirchherr, A. Briel and K. Maeder, *Mol. Pharmacol.*, 2009, **6**, 480–491.
46 L. Josephson, M. F. Kircher, U. Mahmood, Y. Tang and R. Weissleder, *Bioconjugate Chem.*, 2002, **13**, 554–560.
47 M. F. Kircher, U. Mahmood, R. S. King, R. Weissleder and L. Josephson, *Cancer Res.*, 2003, **63**, 8122–8125.
48 O. Veiseh, C. Sun, J. Gunn, N. Kohler, P. Gabikian, D. Lee, N. Bhattarai, R. Ellenbogen, R. Sze, A. Hallahan, J. Olson and M. Zhang, *Nano Lett.*, 2005, **5**, 1003–1008.
49 J. H. Choi, F. T. Nguyen, P. W. Barone, D. A. Heller, A. E. Moll, D. Patel, S. A. Boppart and M. S. Strano, *Nano Lett.*, 2007, **7**, 861–867.
50 W. B. Edwards, W. J. Akers, Y. Ye, P. P. Cheney, S. Bloch, B. Xu, R. Laforest and S. Achilefu, *Mol. Imaging*, 2009, **8**, 101–110.
51 L. Wang, V. Reipa and J. Blasic, *Bioconjugate Chem.*, 2004, **15**, 409–412.
52 A. Burns, H. Ow and U. Wiesner, *Chem. Soc. Rev.*, 2006, **35**, 1028–1042.
53 J. R. Lakowicz, *Principles of Fluorescence Spectroscopy* 2nd edn, Kluwer Academic/Plenum Publishers, New York, 1999.
54 J. T. Lai, D. Filla and R. Shea, *Macromolecules*, 2002, **35**, 6754–6756.
55 J. S. Moore and S. I. Stupp, *Macromolecules*, 1990, **23**, 65–70.
56 G. Sun, C. Cheng and K. L. Wooley, *Macromolecules*, 2007, **40**, 793–795.
57 G. Sun, H. Fang, C. Cheng, P. Lu, K. Zhang, A. V. Walker, J. Taylor and K. L. Wooley, *ACS Nano*, 2009, **3**, 673–681.
58 G. Sun, N. S. Lee, W. L. Neumann, J. N. Freskos, J. J. Shieh, R. B. Dorshow and K. L. Wooley, *Soft Matter*, 2009, **5**, 3422–3429.
59 M. Y. Berezin, H. Lee, A. Walter and S. Achilefu, *Biophys. J.*, 2007, **93**, 2892–2899.
60 Unexpected shoulders were observed in the GPC profile of **II** (ESI† Fig. S1B), at both high and low molecular weights. This observation indicated lower chain transfer efficiency of the mPEG5k macro-CTA, compared with the mPEG2k macro-CTA used for the chain extension to block copolymer **I** (smaller low-molecular-weight shoulder). However, the relatively larger polydispersity of **II** did not affect its assembly behavior and uniform core–shell micelles with narrow size distributions were still obtained.
61 A. B. Lowe and C. L. McCormick, *Prog. Polym. Sci.*, 2007, **32**, 283–351.
62 M. H. Stenzel, *Chem. Commun.*, 2008, 3486–3503.
63 A. W. York, S. E. Kirkland and C. L. McCormick, *Adv. Drug Delivery Rev.*, 2008, **60**, 1018–1036.
64 C. Barner-Kowollik and S. Perrier, *J. Polym. Sci., Part A: Polym. Chem.*, 2008, **46**, 5715–5723.
65 J. M. Harris, ed., *Poly(ethylene Glycol) Chemistry: Biotechnical and Biomedical Applications*, Plenum Press, New York, 1992.
66 *The Handbook: A Guide to Fluorescent Probes and Labeling Technologies* 10th edn, Molecular Probes, Eugene, 2009.
67 G. Sun, A. Hagooly, J. Xu, A. M. Nyström, Z. Li, R. Rossin, D. A. Moore, K. L. Wooley and M. J. Welch, *Biomacromolecules*, 2008, **9**, 1997–2006.
68 The $\lambda_{max,\ abs}$ for **CCFNP2** was shifted to 500 nm, *i.e.*, a 12 nm red-shift.
69 For the PEO_{45}-based PEO-*b*-PVBA system, we have already found that extending of the PVBA block segment length to 26 repeating units causes a dramatic morphological switch from nanoparticles to vesicles.[57] Therefore, the hydrophilic PEO block was replaced with longer PEO_{113} and the hydrophobic PVBA block was correspondingly lengthened to 46 repeating units to retain the block length ratio constant at *ca.* 2.5 (hydrophilic *vs.* hydrophobic).

